Macroscopic Magnetization Control by Symmetry Breaking of Photoinduced Spin Reorientation with Intense Terahertz Magnetic Near Field

Takayuki Kurihara,[1,*,†] Hiroshi Watanabe,[1,‡] Makoto Nakajima,[2] Shutaro Karube,[1,3] Kenichi Oto,[4] YoshiChika Otani,[1,3] and Tohru Suemoto[1,¶]

[1]*Institute for Solid State Physics, The University of Tokyo, 5-1-5 Kashiwanoha, Kashiwa, Chiba 277-8581, Japan*
[2]*Institute of Laser Engineering, Osaka University, 2-6, Yamadaoka, Suita, Osaka 565-0871, Japan*
[3]*Center for Emergent Matter Science, RIKEN, 2-1, Hirosawa, Wako, Saitama 351-0198, Japan*
[4]*Department of Physics, Chiba University, 1-33, Yayoicho, Inage Ward, Chiba-shi, Chiba 263-8522, Japan*

(Received 31 May 2017; revised manuscript received 2 February 2018; published 9 March 2018)

We exploit an intense terahertz magnetic near field combined with femtosecond laser excitation to break the symmetry of photoinduced spin reorientation paths in $ErFeO_3$. We succeed in aligning macroscopic magnetization reaching up to 80% of total magnetization in the sample to selectable orientations by adjusting the time delay between terahertz and optical pump pulses. The spin dynamics are well reproduced by equations of motion, including time-dependent magnetic potential. We show that the direction of the generated magnetization is determined by the transient direction of spin tilting and the magnetic field at the moment of photoexcitation.

DOI: 10.1103/PhysRevLett.120.107202

One of the longest-sought topics in materials science is the manipulation of magnetic order dynamics of condensed matter by light, which is expected to lead to potential applications in ultrafast data recording, spintronics, and quantum computation. Owing to the advancements of femtosecond laser technologies in the last two decades, a variety of laser-based manipulation methods of spin dynamics has been developed, including ultrafast heating [1], spin-polarized carrier excitation [2,3], inverse magneto-optical effects [4–9], optical annealing [10], and terahertz radiation [11–24], to count a few.

In particular, a magnetic field associated with the terahertz radiations has been shown to couple resonantly with the electronic spins through Zeeman interaction [11–17], efficiently driving the magnon dynamics without influencing the electronic ground states. Such an idealistic feature has made terahertz spectroscopy a common tool to study equilibrium and dynamical behaviors of spin order [14,15]. Recent advancements in intense terahertz wave generation technologies have even revealed interesting nonlinear dynamics of magnon in this decisive frequency region [18–22]. In spite of such extensive efforts, however, dynamically changing the magnetization states at a macroscopic level by terahertz waves still remains experimentally unrealized.

On the other hand, magnon dynamics during the optically induced phase transition process has been thoroughly studied in the context of manipulating macroscopic spin order. Since spin states become quite sensitive to external magnetic fields during phase transitions, drastic change of magnetization has been realized with relatively small optical perturbations [5–9]. This suggests that materials that possess intrinsic phase transitions are more suitable candidates for realizing macroscopic spin control with relatively small strength of terahertz radiation than what has been predicted in previous studies [23,24].

Based on this idea, in this Letter, we report the first coherent control of magnetization at a macroscopic level in erbium orthoferrite ($ErFeO_3$) using near-field-enhanced terahertz magnetic fields. Exploiting double pumping by terahertz magnetic fields and optical pulses enabled direct time-domain observation of the dynamics of symmetry breaking process in ultrafast laser-induced spin reorientation phase transition (SRPT) and its coherent control, thereby producing macroscopically magnetized final states with their direction determined by the transient phases of the terahertz magnetic field and the resulting coherent magnons.

The sample used in our study, $ErFeO_3$, is an insulating weak ferromagnet, wherein antiferromagnetically aligned spin sublattices are slightly canted by Dzyaloshinskii–Moriya interaction [25], and exhibits weak ferromagnetic moment $\boldsymbol{M}$. This is a typical material that is known to exhibit a type of magnetic phase transition called spin reorientation. During SRPT, the easy axis of magnetization continuously rotates by 90° from $\boldsymbol{M}//a(\Gamma_2; T < T_L \sim 85\ \mathrm{K})$ to $\boldsymbol{M}// \pm c(\Gamma_4; T > T_H \sim 96\ \mathrm{K})$ due to change in the magnetic anisotropy energy associated with the repopulation of the $4f$ electrons in rare-earth ions [26–28]. Although the SRPT is known to be triggered by various perturbation methods (static magnetic bias, temperature, pressure, optical ionization of rare earths [9], and terahertz electric field [27], etc.), here we utilize a near-infrared femtosecond laser to induce SRPT through ultrafast heating. After photoirradiation, the ensemble average of the final-state magnetization over a

finite volume is usually zero because rotation toward $+c$ and $-c$ directions occurs with equal probabilities. However, this branching ratio can be modified by applying a terahertz magnetic field before the arrival of the optical pump pulse [Fig. 1(a)]. The field ($\boldsymbol{B}_{\mathrm{SRR}}//c$) applied orthogonally to the magnetization ($\boldsymbol{M}//a$) provides torque ($//b$) on magnetization, making the spin to precess [17] around the a axis (1). Because of this coherent precession, symmetry of the $+c$ and $-c$ directions is periodically broken (2). Therefore, the magnetization tends to rotate into either of the two axes upon subsequent photoinduced SRPT process, determined by the transient phase of precession at the moment of arrival of the optical pump pulse (3). As a result, the macroscopically magnetized domain state is expected to appear after the completion of SRPT (4).

Figure 1(b) schematically shows the experimental configuration used in this study. The intense terahertz pulses were generated by optical rectification of Ti:Sapphire regenerative amplifier output using a tilted pulse front technique in a $LiNbO_3$ crystal. It had a half-cycle-like waveform [shown in the Supplemental Material [29] in Fig. S1-1 (a)] with peak electric field up to 300 kV/cm and a temporal duration of subpicoseconds. To obtain sufficient precession amplitude in the first stage, we enhanced the terahertz magnetic field amplitude of the available terahertz source in the near field region using a split-ring-resonator (SRR) metamaterial [16,17]. The SRR structure was designed such that its lowest resonance frequency (f_{SRR}) matched that of the spin precession ($f_{\mathrm{prec}} = 0.06$ THz) at

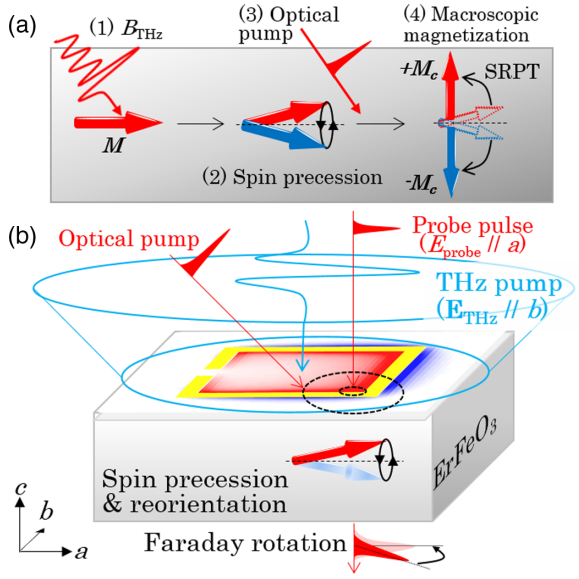

FIG. 1. (a) Schematic illustration of the coherent terahertz magnetic control of macroscopic magnetization using SRPT process. (b) Experimental configuration. The yellow ring indicates SRR structure. The surrounding out-of-plane magnetic field distribution due to circulating current, as calculated by FDTD software, is depicted by a gradient color (red $= B_{\mathrm{SRR}}// + c$, blue $= B_{\mathrm{SRR}}// - c$).

84 K, immediately below T_L. The Q factor of the SRR and peak magnetic field amplitude near the inner corner of the SRR are estimated to be $Q > 15$ and approximately $B \sim 0.1$ T, respectively. The out-of-plane magnetization M_c was probed by the Faraday rotation of transmitted near-infrared pulses. A high quality single crystal of $ErFeO_3$ was grown by the floating zone method [36] with special care on the chemical stoichiometry [29].

The black trace in Fig. 2(a) shows the transient Faraday waveform measured at 84 K after terahertz pulse excitation without an optical pulse. Sinusoidal oscillation corresponds to the spin precession resonantly driven by the SRR. The maximum tilt angle during precession was estimated to be approximately 0.4° from the comparison with total magnetization. In contrast, when we applied an optical pulse, the waveform drastically changed. The red and blue waveforms in Fig. 2(a) show the cases in which we applied an optical pulse with a delay of $dt = 57$ and 63 ps after terahertz excitation. At these delays, the magnetization was slightly tilted to either $+c$ or $-c$ sides. After irradiation by optical pulse, total magnetization was observed to increase by nearly 2 orders of magnitude from the case without optical pumping within 20–30 ps. Following this increase, the signals revealed final states of large finite magnetization that lasted longer than several nanoseconds. The rise time was similar to the previously reported time constant of energy transfer from phonons to $4f$ electrons in the Er^{3+} ion (~20 ps) upon thermalization [7]. Figure 2(b) shows the Faraday signal measured as a function of both probe time t and optical pump time dt, as depicted in a two-dimensional color map. The direction of the final-state magnetization (right graph, hereafter, referred to as the dt waveform) was clearly synchronized with the precession signal. In our experiment, the terahertz pulse excitation alone did not cause SRPT. This means that the effective temperature rise due to dissipation from SRR and direct electronic transitions, e.g., f-f electron transition in Er^{3+} [27,28] by terahertz excitation, is negligible and confirms that the SRPT is induced almost solely by optical pump.

In order to further examine the results, we performed numerical calculation based on the Landau-Lifshitz-Gilbert (LLG) equation, wherein the conventional Hamiltonian $\mathscr{H}(\boldsymbol{S}_1, \boldsymbol{S}_2)$ of antiferromagnetic sublattice magnetizations $\boldsymbol{S}_1$ and $\boldsymbol{S}_2$ was considered [37]

$$\frac{d\boldsymbol{S}_i}{dt} = -\gamma \boldsymbol{S}_i \times \boldsymbol{B}_{\mathrm{eff},i} + \alpha \boldsymbol{S}_i \times \frac{d\boldsymbol{S}_i}{dt} \, (i = 1, 2),$$

where α is the damping parameter and

$$\mathbf{B}_{\mathrm{eff},i} = \frac{d\mathscr{H}(\boldsymbol{S}_1, \boldsymbol{S}_2)}{d\boldsymbol{S}_i}$$

is the effective magnetic field acting on each sublattice spin $\boldsymbol{S}_1$ and $\boldsymbol{S}_2$. The total Hamiltonian $\mathscr{H}(\boldsymbol{S}_1, \boldsymbol{S}_2)$ is given as follows:

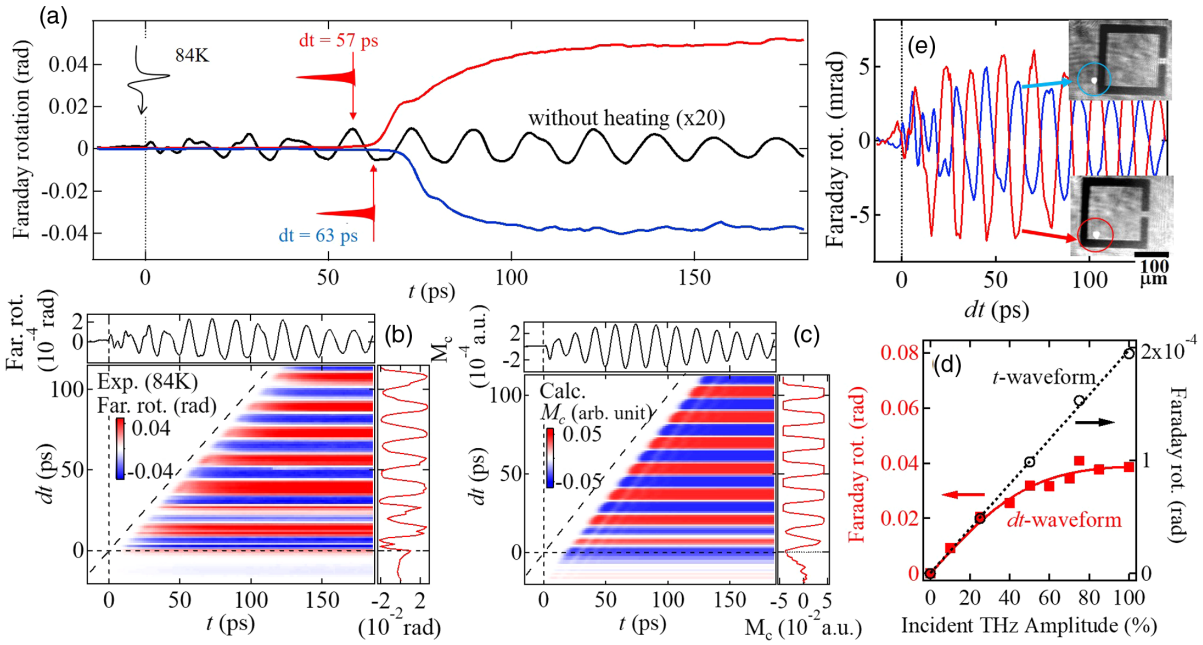

FIG. 2. Experimental results. (a) Faraday waveforms measured at 84 K for typical values of $dt = 57$ ps (red) and $dt = 63$ ps (blue) and measured without an optical pump pulse ("t waveform," black curve). Observed (b) and calculated (c) Faraday signal plotted as a function of t and dt. The top graph (black curve) shows the original spin precession (t waveform), and the right graph (red curve) shows the final value of Faraday rotation plotted against dt ("dt waveform"). (d) Terahertz amplitude dependence of t (black circle) and dt waveforms (red square) measured for fixed probe and pump times at $t = 387$ ps and $dt = 38$ ps. Here, 100% corresponds to a peak terahertz electric field of 300 kV/cm. (e) The dt waveforms measured inside or outside the SRR structure. The inset microscope images show the probe spot positions.

$$\begin{aligned}\mathcal{H}(\boldsymbol{S}_1,\boldsymbol{S}_2) &= J(\boldsymbol{S}_1\cdot\boldsymbol{S}_2)+\boldsymbol{D}\cdot(\boldsymbol{S}_1\times\boldsymbol{S}_2)\\ &+A_{aa}(S_{1a}^2+S_{2a}^2)+A_{cc}(S_{1c}^2+S_{2c}^2)\\ &+A_4(S_{1a}^4+S_{1b}^4+S_{1c}^4+S_{2a}^4+S_{2b}^4+S_{2c}^4)\\ &+\boldsymbol{B}_{\mathrm{SRR}}\cdot(\boldsymbol{S}_1+\boldsymbol{S}_2).\end{aligned}$$

The real-time dynamics of the total magnetic moment $\boldsymbol{M}(t) = \boldsymbol{S}_1 + \boldsymbol{S}_2$ [e.g., Fig. 2(c)] were calculated directly by solving the above equations, assuming realistic values for each of the interaction parameters [29,30,37] (see Sec. S2 of Supplemental Material). Here, the term with $J = 20\ \mathrm{cm}^{-1}$ represents the symmetric exchange interaction, $\boldsymbol{D} = 0.86\ \mathrm{cm}^{-1}$ is the Dzyaloshinskii–Moriya interaction, $A_{aa} = -0.1\ \mathrm{cm}^{-1}$ and A_{cc} (temperature dependent) are the magnetic anisotropy of the second order along the a and c axis, respectively, $A_4 = 7\times10^{-4}\ \mathrm{cm}^{-1}$ is the anisotropy of the fourth order, and B_{SRR} is the terahertz magnetic field. The calculation results [Fig. 2(c)] clearly show macroscopic magnetization alignment synchronized with the terahertz-induced magnon dynamics, in good agreement with the experiment.

While the original spin precession amplitude was almost linearly dependent on the incident terahertz field amplitude, the final-state magnetization clearly saturated at high incident terahertz field strengths [Fig. 2(d)]. The maximum value of generated magnetization, as determined from the value of Faraday rotation, corresponds to the ratio of $+c$- and $-c$-oriented spins reaching up to 82%:18% (see Sec. S3 of Supplemental Material [29]). Considering the finite absorption coefficient (sample thickness $= 100\,\mu$m, $\alpha_{800\ \mathrm{nm}} \sim 2\times10^2\ \mathrm{cm}^{-1}$), this branching ratio would be even higher near the front surface, which undergoes greater heating. Nevertheless, from these facts, it can be unambiguously concluded that a macroscopic amount of magnetization was uniformly aligned toward a selected direction within the photoirradiated area, due to transient symmetry breaking caused by irradiation of SRR-enhanced terahertz magnetic field. When measured inside and outside of the SRR structure [Fig. 2(e)], the sign of the dt waveform was observed to invert. This agrees with the spatial distribution of the out-of-plane magnetic near field B_{SRR} caused by the current circulating in the SRR stripe [16] and clearly indicates that the magnetization alignment was induced by the *magnetic* near field around the SRR structure.

Next, in order to obtain deeper insight into the process of symmetry breaking, we detuned the resonance frequency of the spin system from that of the SRR by changing the sample temperature to 81 K. At this temperature, $f_{\mathrm{prec}} = 0.1$ THz and $f_{\mathrm{SRR}} = 0.06$ THz. Figure 3(a) shows the measured spin precession signal and the corresponding dt waveform. The time window from 115 to 280 ps was expanded to display the most relevant range for discussion. In contrast to the precession in the previous case of 84 K,

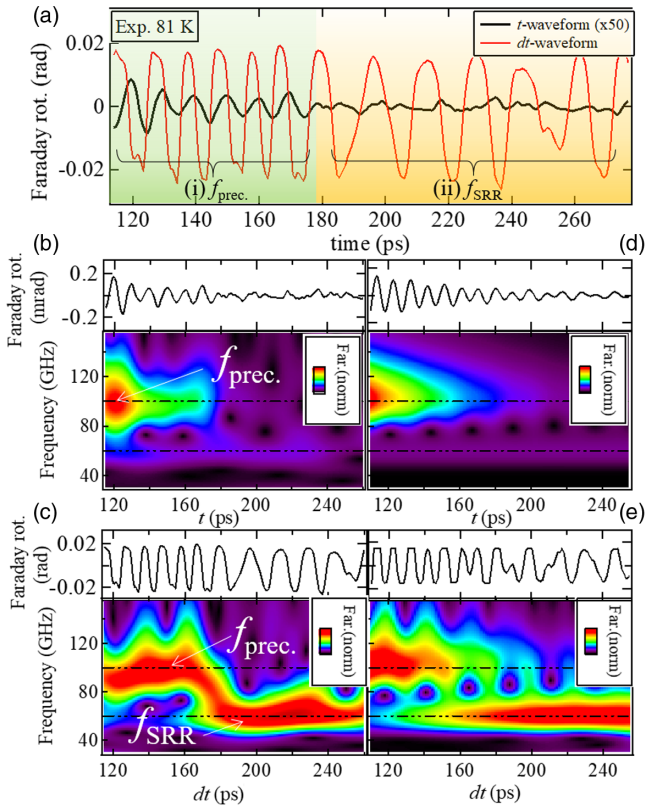

FIG. 3. Faraday waveforms measured or calculated for an off-resonant temperature. (a) Spin precession signal measured at 81 K without optical pump pulse (black), along with the corresponding dt waveform (red). (b),(d) Wavelet transforms of the spin precession measured at 81 K (b) and calculated (d), along with the original waveforms. (c),(e) Wavelet transforms of the dt waveforms corresponding to (b) and (d). The t and dt waveforms shown in (b) and (c) are the same as those in (a). All color scales are normalized within indicated regions.

the precession is off resonant with the SRR and lasts within its original lifetime ($\tau_{\mathrm{prec}} \sim 180$ ps) after terahertz irradiation. This lifetime is shorter than the SRR lifetime ($\tau_{\mathrm{SRR}} > 300$ ps). At an earlier stage of time evolution $t < \tau_{\mathrm{prec}}$ [region (i)], the corresponding dt waveform oscillates at 0.1 THz, the same frequency as the spin precession. In contrast, after $t > \tau_{\mathrm{prec}}$, the amplitude of the 0.1 THz precession component in the t waveform is decayed and only fainter oscillation at 0.06 THz remains [region (ii)], while in the dt waveform, the magnetization is almost saturated and oscillates at 0.06 THz. As observed in the wavelet transformations in Figs. 3(b) and 3(c), the frequency of the dt waveform switches from f_{prec} to f_{SRR} around this delay time $dt \sim \tau_{\mathrm{prec}}$. Similar behavior was reproduced in the results of LLG simulation, as plotted in Figs. 3(d) and 3(e).

The detailed processes of symmetry breaking expected in these two regions are summarized in Figs. 4(a) and 4(b). Judging from their oscillation frequencies, the spin precession signal in the two regions (i) and (ii) is dominated by

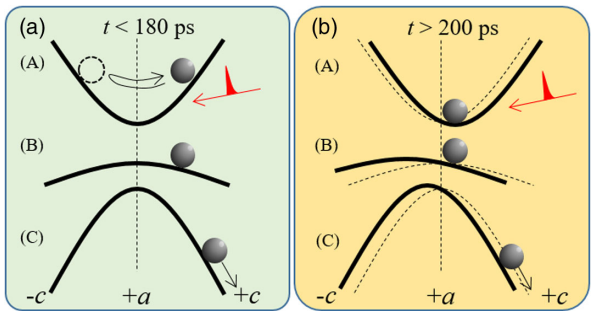

FIG. 4. Dominant processes of symmetry breaking under terahertz magnetic field: Magnetization tilt due to *free* spin precession (a) [region (i) in Fig. 3(a)] and due to *forced* oscillation by off-resonant field excitation (b) [region (ii) in Fig. 3(a)]. The potential curves labeled by the indices (A)–(C) depict the cases before the optical pumping (A), immediately (B) and completely after the curvature change (C). Dotted curves in (b) are the original potential curves in the absence of magnetic field. In (b), the SRR magnetic field is applied toward the $+c$ direction.

the free harmonic oscillation in an anisotropy potential [Fig. 4(a)] and the forced oscillation by the SRR magnetic field [Fig. 4(b)], respectively.

In region (i) [Fig. 4(a) (A–C)], the spin system impulsively excited at the first stage precesses in the potential, at the frequency defined by the potential curvature. Upon photo-induced heating, the curvature continuously changes its sign from positive to negative, making the a axis energetically unfavorable and forcing the macroscopic magnetization to evolve in the $+c$ or $-c$ direction. Therefore, the direction of magnetization in the final state is destined by the transient position of spin system with respect to the crystallographic a axis at the moment of potential curvature change. On the other hand, in the case of region (ii), the free precession is damped and the spin position simply follows the potential minima [Fig. 4(b) (A)], similar to the case of static magnetic field bias. Therefore, the photoinduced magnetization created in this region preserves the direction of the transient SRR magnetic field at the moment of curvature change [Fig. 4(b) (B and C)]. At the time of curvature inversion (B), the potential maxima appears on the opposite side of the a axis from the spin position. This enhances the potential gradient at the position of spin compared to the case without the external field. In other words, at this time, the external terahertz field constructively adds to the internal effective field that acts on the spin to align into the favored direction. Therefore, under the SRR magnetic field, the spin reorientation direction will be firmly determined, even when the real spin tilting angle with respect to the crystallographic a axis is relatively small. This may explain the saturated amplitude of the dt waveform in $t > 200$ ps despite the relatively small amplitude of the spin precession signal compared to that in the $t < 180$ ps region.

It is worth mentioning that the coherent spin precession-induced symmetry breaking model studied in this Letter

was previously proposed in the context of phenomenologically explaining the magnetic domain creation in orthoferrite, with the simultaneous excitation of spin precession and heating by a single circularly polarized optical pulse [6]. However, our experimental scheme to use the terahertz magnetic field separate from the optical pulse enables complete distinction of the two roles and is thus advantageous, allowing for the independent phase control of spin precession and the unambiguous verification of such a model in the time domain.

In conclusion, we succeeded in controlling macroscopic magnetization in $ErFeO_3$ by dynamically breaking the ground state spin symmetry of SRPT with terahertz magnetic near field for the first time, to the best of our knowledge. We obtained the final states reaching over 80% of total magnetization at selectable directions via arrival timing of the optical and terahertz pump pulses. Utilization of the independent pump pulses of terahertz and near-infrared light enabled us to completely distinguish the influence of spin precession from the heat injection, thereby realizing time-domain investigation and phase-dependent control of the symmetry breaking process of SRPT.

From the viewpoint of ultrafast spin control, the combination of our demonstrated concept with the other recently demonstrated novel spin control schemes, such as phonon-mediated crystal field change [38] and direct modification of anisotropy fields by terahertz electric field [27], will also greatly extend the potential applicability of terahertz radiations in this rapidly developing field of ultrafast spintronics. At the same time, the ability to independently manipulate the ground state order dynamics apart from strong optical agitation will be especially advantageous in a variety of photoinduced phase transition materials to disentangle the interplay between different kinds of collective motions.

This work has been partly supported by a Grant-in-Aid for Scientific Research (A) (Grant No. JP23244063) and (B) (Grants No. JP26287060, No. JP25286063, and No. JP16H03886) and a Grant-in-Aid for Scientific Research on Innovative Area "Nano Spin Conversion Science" (Grant No. 26103002) from JSPS (Japan Society for the Promotion of Science). T. K. and S. K. are supported by JSPS through the Program for Leading Graduate Schools (T. K., ALPS; S. K., MERIT). T. K. is thankful for the support from the JSPS Research Fellowship and the JSPS Postdoctoral Fellowship for Research Abroad. M. N. received support from the "Advanced Research Program for Energy and Environmental Technologies" commissioned by NEDO of METI. The authors are grateful for the Materials Synthesis Section in ISSP for the enormous support in crystal growth. We also thank Professor T. Kato in ISSP for insightful discussions and D. Seletskiy at the University of Konstanz for polishing of the manuscript.

*Corresponding author.
takayuki.kurihara@uni-konstanz.de
†Present address: University of Konstanz, Germany.
‡Present address: Graduate School of Frontier Biosciences, Osaka University, Japan.
¶Present address: Toyota Physical and Chemical Research Institute, Japan.

[1] T. A. Ostler *et al.*, Nat. Commun. **3**, 666 (2012).
[2] T. Li, A. Patz, L. Mouchliadis, J. Yan, T. A. Lograsso, I. E. Perakis, and J. Wang, Nature (London) **496**, 69 (2013).
[3] J. A. Gupta, R. Knobel, N. Samarth, and D. D. Awschalom, Science **292**, 2458 (2001).
[4] C. D. Stanciu, F. Hansteen, A. V. Kimel, A. Kirilyuk, A. Tsukamoto, A. Itoh, and Th. Rasing, Phys. Rev. Lett. **99**, 047601 (2007).
[5] A. V. Kimel, A. Kirilyuk, A. Tsvetkov, R. V. Pisarev, and T. Rasing, Nature (London) **429**, 850 (2004).
[6] J. A. de Jong, I. Razdolski, A. M. Kalashnikova, R. V. Pisarev, A. M. Balbashov, A. Kirilyuk, Th. Rasing, and A. V. Kimel, Phys. Rev. Lett. **108**, 157601 (2012).
[7] J. A. de Jong, A. V. Kimel, R. V. Pisarev, A. Kirilyuk, and Th. Rasing, Phys. Rev. B **84**, 104421 (2011).
[8] R. Iida, T. Satoh, T. Shimura, K. Kuroda, B. A. Ivanov, Y. Tokunaga, and Y. Tokura, Phys. Rev. B **84**, 064402 (2011).
[9] D. Afanasiev, A. K. Zvezdin, and A. Kimel, Opt. Express **23**, 23978 (2015).
[10] T. Higuchi and M. K. Gonokami, Nat. Commun. **7**, 10720 (2016).
[11] M. Nakajima, A. Namai, S. Ohkoshi, and T. Suemoto, Opt. Express **18**, 18260 (2010).
[12] T. Kampfrath, A. Sell, G. Klatt, A. Pashkin, S. Mährlein, T. Dekorsy, M. Wolf, M. Fiebig, A. Leitenstorfer, and R. Huber, Nat. Photonics **5**, 31 (2011).
[13] K. Yamaguchi, M. Nakajima, and T. Suemoto, Phys. Rev. Lett. **105**, 237201 (2010).
[14] K. Yamaguchi, T. Kurihara, Y. Minami, M. Nakajima, and T. Suemoto, Phys. Rev. Lett. **110**, 137204 (2013).
[15] K. Yamaguchi, T. Kurihara, H. Watanabe, M. Nakajima, and T. Suemoto, Phys. Rev. B **92**, 064404 (2015).
[16] Y. Mukai, H. Hirori, T. Yamamoto, H. Kageyama, and K. Tanaka, Appl. Phys. Lett. **105**, 022410 (2014).
[17] T. Kurihara, K. Nakamura, K. Yamaguchi, Y. Sekine, Y. Saito, M. Nakajima, K. Oto, H. Watanabe, and T. Suemoto, Phys. Rev. B **90**, 144408 (2014).
[18] M. Shalaby, C. Vicario, and C. P. Hauri, arXiv:1506.05397.
[19] T. Kampfrath, K. Tanaka, and K. A. Nelson, Nat. Photonics **7**, 680 (2013).
[20] Y. Mukai, H. Hirori, T. Yamamoto, H. Kageyama, and K. Tanaka, New J. Phys. **18**, 013045 (2016).
[21] J. Lu, X. Li, H. Y. Hwang, B. K. Ofori-Okai, T. Kurihara, T. Suemoto, and K. A. Nelson, Phys. Rev. Lett. **118**, 207204 (2017).
[22] S. Baierl *et al.*, Phys. Rev. Lett. **117**, 197201 (2016).
[23] A. Pashkin, A. Sell, T. Kampfrath, and R. Huber, New J. Phys. **15**, 065003 (2013).
[24] S. Wienholdt, D. Hinzke, and U. Nowak, Phys. Rev. Lett. **108**, 247207 (2012).
[25] T. Moriya, Phys. Rev. **120**, 91 (1960).
[26] K. P. Belov, A. K. Zvezdin, A. M. Kadomtseva, and R. Z. Levitin, Sov. Phys. Usp. **19**, 574 (1976).

[27] S. Baierl, M. Hohenleutner, T. Kampfrath, A. K. Zvezdin, A. V. Kimel, R. Huber, and R. V. Mikhaylovskiy, Nat. Photonics **10**, 715 (2016).
[28] R. V. Mikhaylovskiy, T. J. Huisman, R. V. Pisarev, Th. Rasing, and A. V. Kimel, Phys. Rev. Lett. **118**, 017205 (2017).
[29] See Supplemental Material at http://link.aps.org/supplemental/10.1103/PhysRevLett.120.107202 for additional experimental and calculation details, which includes Refs. [30–35].
[30] N. Koshizuka and K. Hayashi, J. Phys. Soc. Jpn. **57**, 4418 (1988).
[31] G. V. Kozlov, S. P. Lebedev, A. A. Mukhin, A. S. Prokhorov, I. V. Fedorov, A. M. Balbashov, and I. Y. Parsegov, IEEE Trans. Magn. **29**, 3443 (1993).
[32] S. M. Shapiro, J. D. Axe, and J. P. Remeika, Phys. Rev. B **10**, 2014 (1974).
[33] C. A. Perroni and A. Liebsch, Phys. Rev. B **74**, 134430 (2006).
[34] W. J. Tabor, A. W. Anderson, and L. G. Van Uitert, J. Appl. Phys. **41**, 3018 (1970).
[35] S. R. Woodford, A. Bringer, and S. Blügel, J. Appl. Phys. **101**, 053912 (2007).
[36] A. M. Balbashov, J. Cryst. Growth **52**, 498 (1981).
[37] G. Herrmann, J. Phys. Chem. Solids **24**, 597 (1963).
[38] T. F. Nova, A. Cartella, A. Cantaluppi, M. Först, D. Bossini, R. V. Mikhaylovskiy, A. V. Kimel, R. Merlin, and A. Cavalleri, Nat. Phys. **13**, 132 (2017).